Journal of Scientific & Industrial Research
Vol. 85, May 2026, pp. 383-394
DOI: 10.56042/jsir.v85i5.19101

Variability in Zonal Drift Velocity of Equatorial Plasma Bubbles: A Review

Idahwati Sarudin[1]*, Nurul Shazana Abdul Hamid[2,3]*, Mardina Abdullah[3,4], Suhaila M Buhari[5] & Nur Alia Natasha Johari[1]

[1]School of Physics, Universiti Sains Malaysia, 11800 USM, Penang, Malaysia

[2]Department of Applied Physics, Faculty of Science and Technology, Universiti Kebangsaan Malaysia, 43600 Bangi, Malaysia

[3]Space Science Centre (ANGKASA), Institute of Climate Change, Universiti Kebangsaan Malaysia, 43600 Bangi, Malaysia

[4]Department of Electrical, Electronic and Systems Engineering, Faculty of Engineering and Built Environment, University Kebangsaan Malaysia, 43600 Bangi, Malaysia

[5]Department of Physics, Faculty of Science, Universiti Teknologi Malaysia, 81310 UTM, Skudai, Johor, Malaysia

Received 25 April 2025; revised 22 January 2026; accepted 11 June 2026

The Equatorial Plasma Bubble is a phenomenon occurring in the F-layer of Earth's ionosphere that can disrupt communication and navigation systems. One key aspect of Equatorial Plasma Bubble under active investigation is its zonal drift velocity, which offers an in-depth understanding of plasma behaviour and the natural dynamics of the F-region ionosphere. Previous studies have examined the variations of zonal drift velocity using various tools, including all-sky imagers and radar equipment. This paper aims to review the fundamental theoretical aspects of zonal drift velocity variability across various techniques. It compares zonal drift velocity dependencies based on the aspects considered, highlighting differences in techniques and approaches used in previous studies. Special emphasis is placed on the observation of zonal drift velocity using high-density Global Positioning System network, as this method has consistently demonstrated high performance compared to earlier techniques. Despite decades of investigation, reported EPB zonal drift velocity (V_E) values vary widely across studies which ranging from as low as 0 m/s to over 210 m/s — owing to differences in instrumentation, geographic coverage, and solar activity conditions. A critical gap remains in the systematic cross-comparison of these methods and their accuracy in capturing the full spatiotemporal variability of V_E, particularly in the Southeast Asia sector. This review addresses that gap by synthesising findings from over two decades of V_E studies, identifying consistent seasonal, local time, and solar activity trends, and evaluating the relative performance of each observational approach. The reviewed literature consistently shows that V_E peaks during equinox seasons and high solar activity and decreases from evening (~150–170 m/s) to post-midnight (~20–50 m/s). GPS-based methods using dense receiver networks emerge as the most comprehensive approach, enabling long-term and spatially resolved V_E monitoring.

Keywords: F-layer, Global positioning system, Ionosphere, Longitude, Solar activity

Introduction

Edward Victor Appleton was a scientist who proved the presence of a reflecting atmosphere level. This layer is known as the ionosphere and is detected at altitudes ranging from approximately 100 to 400 km above Earth's surface. The discovery of this layer was made through an experiment known as radio sounding of the ionosphere, using a system called an ionosonde.[1] Since the early 20th century, the ionosphere has been extensively studied using various methods, including not only ionosondes but also rocket and satellite measurements.[2] More recently, researchers have employed the Global Positioning System (GPS) to study the ionosphere behaviour across the whole world. These advancements in measurement techniques highlight the significant influence of the ionospheric layer on the propagation of radio waves.[3]

The configuration of the magnetic field that interacts with Earth's surface results in significant ionospheric plasma depletion in regions near the equator during the night time. This poses a notable challenge for satellite-based navigation and communication systems, as radio signals passing through these irregularities encounter disruptions. These irregularities, known as ionospheric plasma bubbles in the equatorial area, are also named as Equatorial Plasma Bubbles (EPBs), or Equatorial Spread F (ESF).[4] The initial measurements of ESF date back to the late 1930s and were conducted using an ionosonde.[5] Subsequently, various instruments have been employed to observe and quantify EPBs. The choice of observing instruments has led to

*Authors for Correspondence
E-mail: idahwati@usm.my; zana@ukm.edu.my

different terminologies being introduced for these phenomena, including depletions, wedges and plumes. Nevertheless, all these terms are linked to the similar mechanism known as the Rayleigh-Taylor Instability (RTI).[6] This study specifically focused on EPBs observed using GPS data.

Investigating the characteristics of EPBs is crucial for maintaining smooth communication between satellites and receivers. The properties of these irregularity scale lengths are of special importance as they can significantly impact the functionality of satellite-based communication and navigation systems by diminishing signal strength and perhaps resulting in signal lock loss.[7] Observations of EPB characteristics have been conducted using ground-based instruments and satellites. This paper focuses on the EPB characteristic known as the eastward drift velocity (zonal velocity). By investigating he irregularity drifts in the F-layer, a deeper understanding of plasma properties and the natural dynamics in the F-layer of the ionosphere can be achieved.[4] The influence of wind strength on zonal velocity can be clearly understood from a recent study that was conducted by Sarudin *et al.*[8] by classifying the observations into two categories according to wind strength: strong and weak winds on separate nights. Pre-Reversal Enhancement (PRE) was responsible for the successful reporting of the onset time and location of EPBs at 1320 UT (2120 LT) and 100° (500 km) longitude. In the past few decades, zonal drift velocity (V_E) in the F-layer has been extensively studied using various observational tools such as All-Sky Imagers (ASI)[9–12] and radar.[13–15] Past studies have indicated that during quiet conditions, EPBs move eastward, in line with the direction of the neutral wind. Additionally, the characteristics of V_E in the F-layer were first discussed by Ronald Francis Woodman[16] in 1970, where he noted that the daytime pattern of V_E is westward but shifts to eastward at night. Most of the investigations have focused on the east-west motion of EPBs in geomagnetic coordinates. This focus stems from the idea that EPB motion coincides with the geomagnetic flux tube. Thus, the V_E is influenced by the geomagnetic flux tube, which is determined by various ionospheric parameters.

Moreover, many earlier studies primarily analysed irregularity drifts by using imaging techniques[10,17–19] and subsequently associated V_E with zonal neutral wind velocity (w) which were obtained using ground-based instruments known as Fabry-Perot Interferometers (FPI).[9,20–22] Chapagain *et al.*[20] in their study examined equatorial latitude data and found similar patterns in the day-to-day variations of both zonal neutral wind with V_E. They observed that during the evolution of EPBs in the evening, w was higher than V_E, indicating that the F-layer dynamo might not be fully active. In a later study in geomagnetically conjugate observation of plasma bubbles, Fukushima *et al.*[21] analysed data from stations in Kototabang, Indonesia and Chiang Mai, Thailand, reporting that their findings demonstrated local time variations for w which were consistent with variations in V_E. Additionally, other studies have reported results from modelling the interactions between plasma drift in the ionosphere and neutral wind motion. One such study by Chapagain[23] demonstrated that even though the variation patterns in the drift of plasma model and motion of wind are aligned, the magnitudes of the V_E obtained differ. Previous research has compared the identified EPB V_E with the Rate of Total electron content change Index (ROTI), where Total Electron Content (TEC) represents electron content. However, these comparisons are limited by the availability of broad network and thermospheric neutral wind data from Fabry-Perot Interferometers (FPI). Therefore, this paper attempts to present a comprehensive analysis of past studies that utilised a high-density GPS receiver network in the observation of EPB V_E. Despite the growing body of research on EPB V_E, a critical research gap persists are the existing studies that are largely method-specific, region-specific, or limited to short observation windows, making it difficult to compare results across techniques and geographic sectors. In particular, the Southeast Asia (SEA) region which characterised by its unique longitudinal and geomagnetic configuration that remains underrepresented in comprehensive V_E reviews. Furthermore, the relative reliability and accuracy of different observational methods have not been systematically evaluated. This review addresses these gaps by critically comparing the methods, geographic coverage, and reported V_E ranges from previous investigations, with emphasis on high-density GPS networks as an emerging gold standard. The specific objectives of this review are: (i) to compare observational techniques used for EPB V_E measurement; (ii) to identify temporal and spatial patterns of V_E across different regions, with particular focus on SEA; (iii) to evaluate the influence of solar activity, season, local time, and longitude on V_E; and (iv) to assess the advantages and limitations of GPS-based methods relative to conventional instruments such as ASI and radar.

The next section of this work examines the contributions of different methodologies to the observation of the EPB structure after providing a quick introduction to EPB and its V_E. This is then followed by an explanation of the variations in EPB occurrences which were attributed to several factors. An in-depth and detailed examination of the EPB V_E, including the determination of EPB V_E, is presented in the third section. This subsequently leads to a discussion of EPB zonal drift velocity variations in relation to season, Local Time (LT), and Solar Activity (SA) levels in the last section.

Observations of Zonal Velocity of EPBs

EPB Structure Observations

Since the beginning of the investigation into EPB structure, various instruments have been developed for the observation, including the ionosonde[24,25], Equatorial Atmosphere Radar (EAR)[26–29], imaging techniques using All Sky Imager (ASI)[10,19,30,31] and measurements from in-situ satellites.[32–36] Another study[36] identified the unique combinations of differently shaped EPB that occurred within a small longitude. However, each equipment has limitations in spatial and temporal resolution. In this review, the emphasis is on observations of EPB utilising high-density GPS receivers as the presence of an extensive network enhances the clarity of the observed EPB structures, thus facilitating more accurate determinations of the EPB V_E.

EPB was first discovered through an ionosonde experiment conducted by Booker and Wells[5] in 1938. The test was conducted to measure the height of the E-layer, F1-layer, F2-layerand other parameters. In the study, Booker and Wells[5] discovered that the measurement of the height of the layers could not be performed due to frequency dispersion that occurred. By contrast, EPB observation using ASI relies on the detection of radiant light in the 630.0 nm spectrum released by oxygen ions at an altitude of around 250 km. ASI features a 1000 km-diameter circular aperture (Field of View, FOV). The decrease in brightness, which is proportionate to the amount of electrons at the reported altitude, is used to identify the presence of EPB. The reduction in airglow appears as a dark region that can be observed using an ASI filter with a wavelength of 630 nm. Observations using ASI and those from GPS data have been compared to verify the ability of GPS data in determining the EPB V_E.[37] However, ASI can only operate on dark nights without moonlight and the presence of clouds.

Variations in EPB Presence

Variation in the presence of EPB has been studied and reported in previous studies using various observational equipment. Among the observation equipment and techniques used to investigate EPB presence are ionosondes[24,25] and in-situ satellite measurements.[35] Previous researchers have reported that variations in the plasma bubbles observed depend on several factors, including local time[12,38] latitude and longitude[32, 39], solar activity levels[40–42] and season.[43–46] Variations in EPB presence peak at dusk over time, which is consistent with the time EPB is first observed at the geomagnetic equator. EPB then rises to higher latitudes via conduction along the magnetic field flux tube EPB presence levels vary according to the latitude and longitude of the observation area. Based on past studies, Gentile *et al*.[32] found that EPB presence levels in the Atlantic are the highest compared to other sectors in Asia, the Pacific, and Africa. Additionally, EPB presence levels in the SEA sector (90°N–120°N) reach their maximum around March and September, as reported by Nishioka *et al*.[39] using GPS receivers from a global network. In contrast, EPB levels in the Atlantic and African sectors peak in April and October. This shows that the variation in EPB presence also depends on seasons, as explained by Ronald Tadayoshi Tsunoda[47] that focused on the growth phase of EPB. During the equinox, the boundary between day and night is parallel with the magnetic field flux, causing an increase in plasma conductivity within the magnetic field's polar flux and subsequently raising the EPB presence levels. Consequently, EPB presence is found to peak during the equinox season in longitude range from 169° W to 26° E.[39,47–50]

Findings regarding variations in EPB presence with season and solar activity levels in SEA for the period of 2008–2013 are illustrated in Fig. 1.[(49)] The plasma bubbles observed has reached its peak in March/April and September/November, coinciding with the equinox seasons. Conversely, the lowest EPB

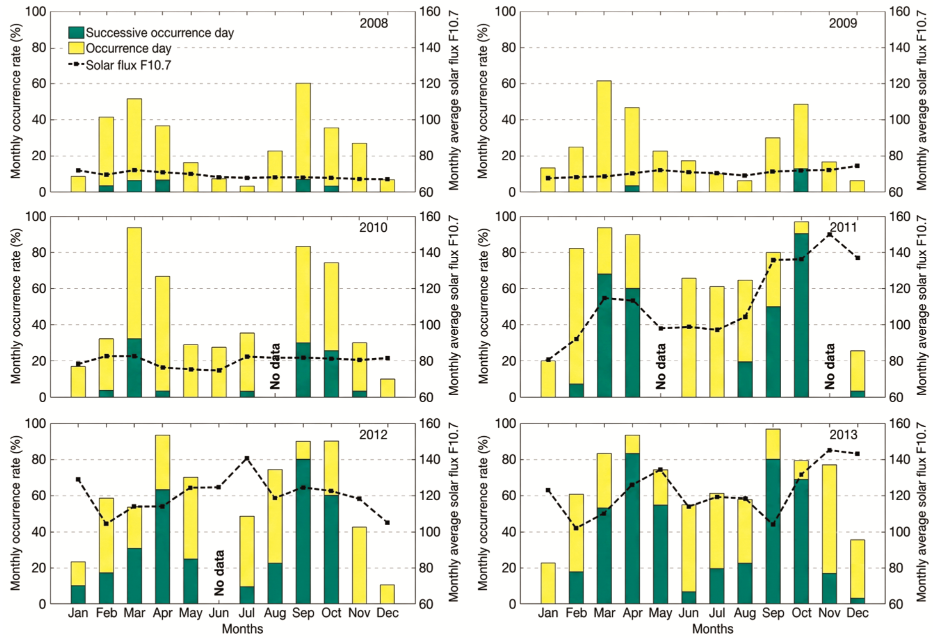

Fig. 1 — EPB occurrence rate from 2008 to 2013 in Southeast Asia. Reproduced from Buhari *et al.*[49]

presence occurred in solstice season: December–January and June–July. Between 2010 and 2013, the mean solar flux index for those months showed an increase in solar activity, which coincided with a steady increase in the rate of EPB presence to over 90%. Independent studies in India[30,51], America[52], the Atlantic and Africa[32,39], and various regions, including Africa, Asia, the Eastern Pacific, the Atlantic and Central Pacific, as well as India have also identified that the presence of EPB is consistently correlated with solar activity levels. Despite numerous in-depth studies, researchers have yet to definitively verify and explain the underlying trigger for the occurrence of EPB.

Determination of EPB's Zonal Drift Velocity

This study aims to assess the variation of V_E which is important for understanding plasma and neutral dynamics in the ionospheric F-layer.[4] Preliminary studies show that under geomagnetically quiet conditions, V_E moves in an easterly (E) direction, which aligns with the neutral wind direction. Since EPB movement is thought to be parallel to the geomagnetic field lines, the majority of independent investigations have concentrated on EPB migration in the E direction towards the geomagnetic west (W). Ronald Francis Woodman[16] used the EAR at Jicamarca, Peru, to investigate the properties of V_E at the magnetic equator for the first time in 1970. Ronald Francis Woodman's[16] study revealed that during the day, the wind flow cycle is in the W direction but suddenly changes to the E direction at night. Since then, numerous studies on the relationship between V_E and the wind, geomagnetic activity, and solar irradiance have been conducted.[53–55]

In the past few decades, the determination of V_E in the F-layer has been widely carried out using imaging techniques[10–12,17,18,30,38,53] with most of the studies conducted using ASI observation. Additionally, the irregularity drifts observed by another alternative technique involves the use of radar as demonstrated in Indonesia.[56] The results of the cross-section analysed can be seen in Fig. 2. The cross-sections of Ascension Island (left) from April 4–5, 1997, and Christmas Island (right) from September 28–29, 1995, were taken in the W–E direction (positive eastward). Both measurements were taken during periods of Low Solar Activity (LSA) using the same ASI camera. The plot compares the evolution, development, spread, and V_E between the two locations. The dark band (EPB) moves from the lower left to the upper right (i.e., from W to E over time), as can be observed from the arrows. The small scatter as seen in the Ascension Island plot indicates a smaller V_E, while the EPB observed at Christmas Island is considerably large due to its almost linear scatter, illustrating that the EPB moves with a high and stable V_E throughout the night.

In a previous work by Otsuka *et al.*[56], V_E was estimated utilising imaging techniques as well as observation data using the EAR from three single-frequency GPS receivers positioned at Kototabang,

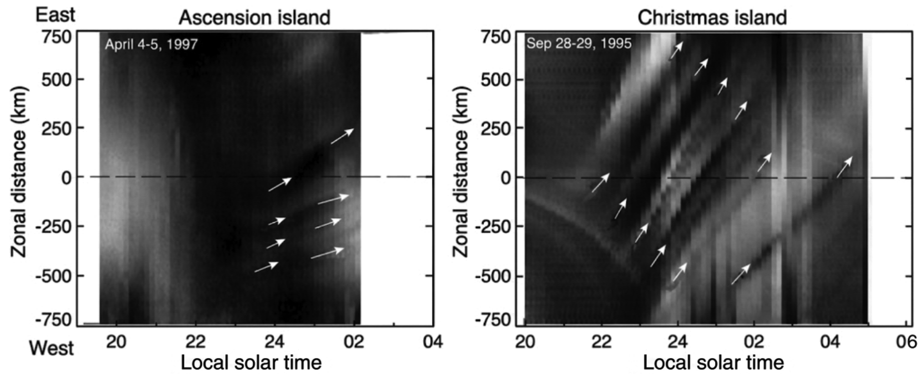

Fig. 2 — Cross-section in the W to E direction (positive E direction) for (left) Ascension Island and (right) Christmas Island; The dark path represents the EPB, while the arrows indicate its movement direction; Reproduced from Chapagain *et al.*[17,18]

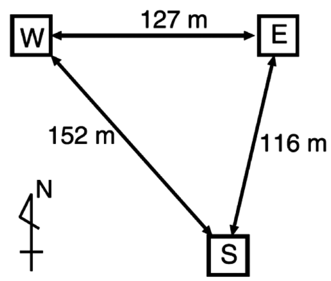

Fig. 3 — Configuration of three GPS receivers installed at KTB, Reproduced from Otsuka *et al.*[56]

Indonesia (KTB) (0.20 S, 100.32 T; geomagnetic latitude 10.6 S). The GPS signals were sampled by the GPS receivers at a frequency of 20 Hz. The three receivers were separated by 116, 127, and 152 meters, respectively. The third receiver was situated in relation to the S, while the other two (E and W) were geographically aligned. The configuring of the three GPS devices is shown in Fig. 3.

The signal observability captured using the three GPS receivers was recorded over time variations on 23 March 2004 (Fig. 4a). Strong fluctuations in signal observability, referred to as scintillations, (indicating the presence of EPBs), were observed between 2025 and 2220 hours LT. The signal observability over time variations of one minute during the strong scintillations observed between 2053 and 2054 hours LT showed in Fig. 4b. The disturbances in signal observability observed from the three GPS receivers (E, W and S) were considerably similar, but there was a slight time lag between the receivers. The disturbance observed on the E side was slightly delayed compared to the receiver on the W side. This suggests that the disturbance in the ionosphere causing the scintillation is moving towards the E side. To quantitatively measure the time lag, a correlation technique was applied to obtain the variations of signal observability over one minute. In another study[56], V_E is determined as the time of maximum correlation between the signal observability perceived by the receiver. The V_E value is considered equivalent to the rate of plasma movement, if the disturbance moves without any change in its structure during observation.

EPB Zonal Drift Velocity Variation

The climatology V_E or speed of EPB has been studied using various measurement equipment, including the EAR[19,57], ASI[12,30] and in-situ satellite measurements.[35] The range of EPB V_E values that was measured using different equipment were listed in Table 1. It also summarises the information regarding the region and observation period of each study. There is relationship of EPB behaviour with various factors.[19] The EPB V_E variation was identified based on distinct factors such as solar activity, longitude, season and local time. According to Barros *et al.*[9] the V_E value of plasma bubbles observed at Earth's equator was 123 m/s, decreasing to 65 m/s at 35°S latitude. Another study by Pimenta *et al.*[45] concerning longitudinal effect on EPB V_E found the values of EPB V_E at the equator and 19°S latitude were 160 m/s and 150 m/s, respectively. Basu *et al.*[4] demonstrated that V_E was also influenced by local time, reporting that the initial V_E at 2100 hours LT of 150 m/s decreased to 50 m/s at 0100 hours LT. Similarly, when studying high altitude plasma bubbles observed at the geomagnetic conjugate locations, Shiokawa *et al.*[31] found that EPB V_E dropped from 170 m/s in the evening to 28 m/s by midnight. Meanwhile, Yao and Makela[12] in their study of EPB zonal drift V_E in the pacific region by imaging-based investigation confirmed the effect of SA level and season son EPB V_E during quiet conditions. They found that V_E was

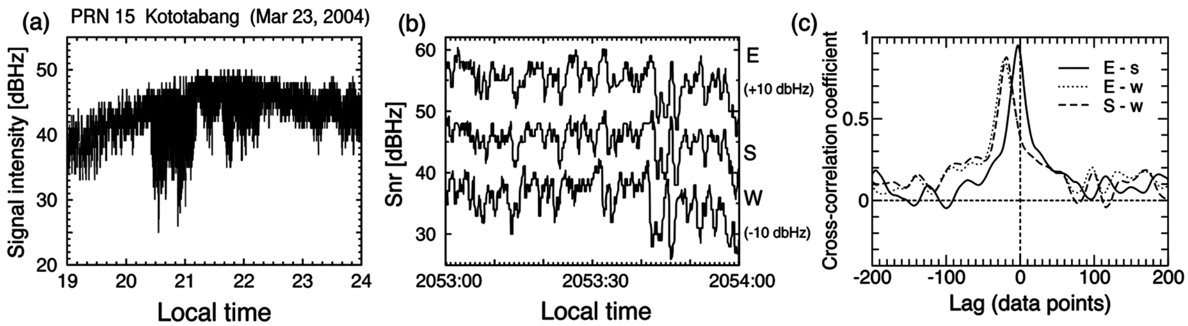

Fig. 4 — (a) Observation of signals captured from a GPS satellite (PRN 15) at KTB between 1900 and 2400 hours LT on 23 March 2004; (b) Observation of signals picked up by three short-range GPS receivers over one minute between 2053 and 2054 hours LT on 23 March2004; and (c) Cross-correlation coefficient between the signal intensity observed by the three receivers; Modified based on Otsuka *et al.*[56]

Table 1 — Summary of reviewed studies on EPB zonal drift velocity variation by using various equipment

Observation equipment	Region	Observation period	Range of EPB zonal drift velocity, VE (m/s)
ALTAIR radar[15]	Roi-Namur, Marshall Island	24 July 1979	0–40 (based on the local time, LT) 0 at 1947 LT to 1040 LT 10 at 1940 LT 30 at 1925 LT 40 at 1855 LT
630 nm airglow[13]	Vanimo, Papua New Guinea	16/17 April to 4/5 November 1980	90–140
Spaced-receiver scintillation and radar interferometer[4]	Huancayo and Jicamarca, Peru	11 October 1988 – 12 October 1988	50–150 (based on the local time, LT) 150 at 2100 LT 50 at 0100 LT
630 nm airglow[22]	Kolhapur, India	March 1993 - January 1994	143–200 during geomagnetically quiet nights
GPS receivers and 630 nm all-sky images[53]	Cachoeira Paulista, Brazil	December 1998 – February 1999	140–160 (based on the local time, LT) 160 at 2000 LT 140 around midnight
Far-Ultraviolet Imager (FUV) [58]	Jicamarca, Peru	2002 to 2004	170–210 (based on the solar activity level) 170 during MSA level 210 during HSA level
630 nm all-sky images[45]	Sao Joao do Cariri and Cachoeira Paulista, Brazil	December 1999 to February 2000	150–160 (based on Earth's latitude and the local time, LT) 150 at 19° S latitude (2000 to 2200 LT) 160 at equator (2100 to 2200 LT)
Two 630 nm airglow[31]	Sata, Japan and Darwin, Australia	4 April 2002	28–170 (based on the local time, LT) 170 at 2000 to 2100 LT (evening) 28 at 2300 to 0000 LT (midnight)
All-sky imagers (ASI) and 47-MHz Equatorial Atmosphere Radar (EAR) [56]	West Sumatra, Indonesia	2003 to 2004	150–50 at 1940 LT to 0010 LT (March to April 2003) 130–80 at 1940 LT to 2340 LT (September to October 2003) 140–65 at 2020 LT to 0110 LT (March to April 2004) 120–70 at 2020 LT to 2310 LT (September to October 2004)
OI 630 nm scanning photometer airglow[59]	Cachoeira Paulista, Brazil	October to March, from1980 to 1994	95.3–116.6 (based on F10.7) 116.6 at F10.7 = 250 sfu 95.3 at F10.7 = 100 sfu

(*Contd.*)

Table 1 — Summary of reviewed studies on EPB zonal drift velocity variation by using various equipment (*Contd.*)

Observation equipment	Region	Observation period	Range of EPB zonal drift velocity, VE (m/s)
Airglow images[38]	Sao Joao do Cariri, Brazil	September 2000 to April 2007	20–65 (based on the local time, LT) 40 at 1800 LT 65 at 2200 LT 20 at 0500 LT
GNSS receivers[9]	South America	November 2012 and January 2016	65–123 (based on Earth's latitude) 65 at 35° S latitude 123 at equator
All-sky CCD airglow imager[10]	Christmas Island, the Pacific Ocean (2000 km due south of Hawaii)	15 September 1995 to 3 October 1995	80–100 (based on the occurrence time) 90–100 at midnight ~ 80 post-midnight
OI 630 nm airglow all-sky images and GPS scintillation receivers[11]	Boa Vista (BV) and Campo Grande (CG), Brazil	October 2002 and November 2002	35–95 at BV 73–114 in BV (theoretical) 31–104 at CG 92–137 in CG (theoretical)
Cornell Narrow Field Imager (CNFI)[17]	Island of Maui, Hawaii (the Pacific)	2002 to 2005	Quiet day: 20–100: Equinox, high flux 40–80: Equinox, low flux 22–76: Solstice, high flux 30–80: Solstice, low flux Active day: 40–96: Equinox, high flux 30–78: Equinox, low flux 38–83: Solstice, high flux 28–78: Solstice, low flux
OI 630 nm emission[17,18]	Northeastern Brazil	October to December, from 2009 to 2010	~100–175 from ~1830 LT to 2130 LT
OI 630 nm emission[20]	Peru	March 2011 to March 2012	Solar flux ~100 and 140 sfu: 10–170 Solar flux ~ 90 and 123 sfu: 10–125
Communication/ Navigation Outage[60] Forecasting System (C/NOFS)	Jicamarca, Peru	May 2008 to April 2014	60–120 at 2000 to 2200 LT 40–100 at 2200 to 0000 LT 20–70 at 0000 to 0200 LT 15–50 at 0200 to 0400 LT
GNSS systems[61]	Brazil	July 2014 to July 2015 and July 2019 to July 2020	Equatorial: 100–108 in LSA 120–130 in HSA Low latitude (20° S): 90 in LSA 120 in HSA
GNSS TEC/Scintillation receivers, VHF coherent radar and ionosonde[62]	East and Southeast Asia	July 2022	Quiet day: Upward drift: 33 Eastward drift: 20 (initial phase) Westward: 100 (decaying phase) Active day: Upward drift: 17

highest, ranging from 40 m/s to 96 m/s, during the equinox and high solar flux, while it was lowest, ranged from 28 m/s to 78 m/s, during the solstice and low solar flux.

A critical examination of the studies summarised in Table 1 reveals several important methodological distinctions. Broadly, the reviewed studies can be categorised into three groups: (i) ground-based optical imaging methods (630 nm airglow and ASI), which offer good spatial resolution but are limited by weather conditions and restricted to night-time observations; (ii) ground-based radio and radar techniques (including ionosondes, EAR, spaced GPS receivers, and scintillation receivers), which allow continuous monitoring but are generally constrained to fixed geographic locations; and (iii) satellite-based in-situ measurements (e.g., C/NOFS, FUV imager), which provide global coverage but lower spatial resolution and are subject to orbital sampling limitations. GPS-based methods using dense receiver networks represent a fourth, hybrid category that combines spatial breadth with high temporal resolution and have demonstrated strong agreement with results from traditional imaging techniques. In terms of accuracy, satellite and GPS-based studies tend to report more consistent and repeatable V_E estimates, whereas single-station optical methods show higher night-to-night variability. Notably, studies using high-density GPS networks such as Sarudin *et al*. (2020) for SEA have enabled more robust identification of V_E patterns across multiple solar cycles and seasons, addressing a key limitation of earlier single-event or short-duration studies. However, each approach carries inherent uncertainties: optical methods are sensitive to sky transparency and calibration; radar methods rely on assumptions about scatterer morphology; and GPS-derived V_E depends critically on network density and the algorithm used to track EPB propagation.

Past studies have focused a variety of instruments to examine how solar activity, season and local time affect V_E fluctuations. An example is the study by Otsuka *et al*.[56] which was conducted using GPS data from the KTB station which relied on ground and satellite measurements. The study, which considered data collected during the equinox season, reported that the V_E is 10 to 20 m/s higher in March–April compared to September–October during Moderate Solar Activity (MSA).However, the findings from the study may not provide a comprehensive assessment as the researchers only focused on one level of solar activity which is MSA. Therefore, additional investigations that include both low and high solar activity levels are necessary to gain complete understanding of the influence of solar flux.

In addition to studies on the seasonal dependence of V_E, previous research has also linked V_E to local time and solar activity levels. For example, the study

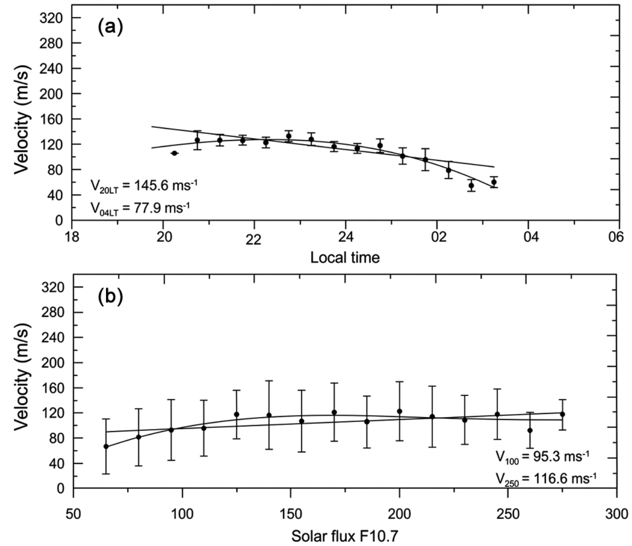

Fig. 5 — Variation of V_E in relation to (a) local time and (b) solar flux F10.7; Modified based on Terra *et al*.[59]

by Terra *et al*.[59] analysed 109 nights of data from the Brazilian sector and found that V_E decreases with increasing time. As shown in Fig. 5a, the V_E ranged from 145.6 m/s at 2000 LT to 77.9 m/s at 0400 LT. Even though this finding might not be comprehensive due to the short research period (the duration of 109 nights only covered LSA and HSA), it still aligns with the results of other studies.[38,51] The variation of V_E also tends to increase with rising solar activity. As shown in Fig. 5b, the values of V_E increased from 95.3 m/s during LSA to 116.6 m/s during HSA. The plasma within the ionosphere is mostly driven by the electric field produced by the dynamo of the E and F-layers.[63] The F-layer dynamo is completely activated during HSA. However, because the plasma density is reduced during LSA, it is not completely activated. Stronger winds result from the greater pressure decreases caused by sun heating during HSA. As a result, during HSA periods, V_E levels are higher.

Furthermore, an early investigation by Terra *et al*.,[59] also discovered the peak of Electron Density Variation (the highest value of V_E) occurs before night time. This finding of V_E peak has also been reported by several past studies.[12,38] However, the exact timing of the V_E peak remains uncertain, as past research reported this peak within a broad estimated period of three to four hours. The dependence of V_E on solar activity levels, local time and season is still inadequately comprehended because of previous studies' restricted access of long-term data. Therefore, utilising a high-density GPS network in the recent study by Sarudin *et al.*,[37] would enable a comprehensive analysis of the long-term variation of V_E, while also allowing for precise identification of the V_E peak timing.

A cross-study synthesis of the V_E values compiled in Table 1 reveals a consistent set of trends across different observational platforms. Evening EPB drift velocities (around 2000–2100 LT) are typically in the range of 100–175 m/s, progressively decreasing to 15–50 m/s in the post-midnight sector, regardless of method used. This local time dependence is robustly confirmed across optical, radar, satellite, and GPS studies. Similarly, the enhancement of V_E during HSA compared to MSA and LSA is consistent across all instrument categories, with GPS and satellite studies reporting the most systematic documentation of this trend over multi-year datasets. Seasonal patterns also converge across methods: V_E peaks during equinox months (particularly March–April and September–November in the SEA sector) and is suppressed during solstice periods. However, the absolute V_E magnitudes reported across studies vary considerably, partly reflecting genuine geographic and solar cycle differences, and partly reflecting methodological uncertainties. For optical methods, uncertainties arise from cloud cover, calibration variability, and the spatial averaging inherent in wide-field imagers. Radar-based methods carry uncertainties related to assumptions about the isotropy of scatterers and signal-to-noise ratios. GPS-derived V_E uncertainties depend on network density, inter-receiver baseline length, and the propagation tracking algorithm employed. Satellite in-situ measurements, while globally distributed, may mistake spatial structures for temporal variations due to orbital motion. Several reviewed studies acknowledge limited observation windows that span only one or two solar cycles, restricting their ability to capture long-term trends. Additionally, most single-station studies cannot distinguish between longitudinal and temporal effects on VE, since they observe only a fixed geographic point. The limited availability of concurrent neutral wind data (e.g., from FPIs) in most regions also constrains the interpretation of V_E drivers, particularly in assessing the relative roles of E-region and F-region dynamo processes. Víctor Navas-Portella *et al*. (2024) further highlighted the importance of incorporating high-resolution GPS networks to bridge these observational gaps, demonstrating that denser networks markedly improve the spatial characterisation of EPB drift. Together, these considerations underscore the value of multi-instrument and multi-site approaches for achieving reliable, reproducible V_E estimates.

Conclusion

This review highlights the importance of studying EPBs to better understand their behaviour and the dynamics of the F-layer ionosphere. The V_E is a key characteristic of EPBs, and this review has comprehensively explored existing research on V_E measurement and analysis. Studies utilising high-density GPS receivers have demonstrated good agreement with other similar methods of estimating V_E. Furthermore, this review has successfully presented research utilising high-density GPS networks to estimate V_E, revealing its variations based on solar activity levels, season and local time. Among the reviewed methods, high-density GPS networks emerge as the most effective approach for long-term, spatially resolved V_E monitoring, offering all-weather operability and broad geographic coverage that single-station optical or radar methods cannot match. ASI and airglow imaging methods remain valuable for their high spatial detail and direct visualisation of EPB morphology but are inherently limited by weather and lunar conditions. Radar-based observations provide robust V_E estimates at fixed equatorial stations but are geographically sparse. Satellite in-situ techniques offer the only truly global perspective but suffer from temporal aliasing. What remains unclear from the existing literature is: (i) the precise trigger mechanism linking PRE strength to V_E magnitude on a night-to-night basis; (ii) the relative contribution of E-region versus F-region dynamo processes to V_E variability; and (iii) the extent to which ionospheric forcing from lower atmosphere wave activity (gravity waves, atmospheric tides) modulates V_E. Future research should prioritise: (i) the deployment and coordination of multi-instrument networks in data-sparse regions such as SEA, Africa, and the Pacific sector; (ii) development of standardised cross-method validation protocols to enable direct comparison of V_E values obtained by different techniques; (iii) long-term GPS studies spanning multiple solar cycles to better characterise V_E climatology under varying solar and geomagnetic conditions; (iv) integration of neutral wind measurements (e.g., from FPI networks) with GPS-derived V_E to improve understanding of plasma-wind coupling; and (v) application of machine learning approaches to identify complex, multi-factor relationships governing V_E variability that may not be captured by traditional statistical analyses.

Conflict of interest

The authors declare no competing interests.

Acknowledgement

The authors thank the Universiti Sains Malaysia through Bridging Grant with project number R501-LR-RND003-0000001578-0000 and the Fundamental Research Grant Scheme (FRGS) under the Ministry of Higher Education (KPT) Malaysia, with the grant code number FRGS/1/2023/STG07/UKM/02/1.

Author Contributions

Idahwati Sarudin provided the idea of writing a review paper and contributed to reviewing and editing the draft. Nurul Shazana Abdul Hamid, Mardina Abdullah, Suhaila M. Buhari, and Nur Alia Natasha Johari critically revised the draft for important intellectual content. All authors contributed to the article and approved the final version for submission.

References

1 Beynon W J G, sir Edward Appleton: an appreciation, *Phys Bull*, **16(8)** (1965) 317–318.

2 Evans J V, Satellite beacon contributions to studies of the structure of the ionosphere, *Rev Geophys*, **15(3)** (1977) 325.

3 Bahari S A, Abdullah M & Hasbi A M, A review of ionospheric studies in Malaysia using GPS, *IEEE Int Conf Space Sci Commun (Icon Space)*, **(2015)** 95–100.

4 Basu S, Kudeki E, Zengingonul H P, Biondis M A & Meriwether J W, Zonal irregularity drifts and neutral winds measured near the magnetic equator in Peru, *J Atmos Sol Terr Phys*, **53** (1991) 743–755.

5 Booker H G & Wells H W, Scattering of radio waves by the F-region of the ionosphere, *Terr Magn Atmos Electr*, **43(3)** (1938) 249–256.

6 Kelley M C, *The Earth's Ionosphere: Plasma Physics and Electrodynamics*, **43** (1989).

7 Bhattacharyya A, Equatorial plasma bubbles: A review, *Atmosphere*, **13** (2022) 1637.

8 Sarudin I, Abdul Hamid N S, Abdullah M, M Buhari S, Otsuka Y, Perwitasari S & Yatin C, Equatorial plasma bubble onset during strong and weak neutral winds over Southeast Asia, *J Kejurut*, **36(3)** (2024) 1281–1289, https://doi.org/ 10.17576/jkukm-2024-36(3)-36.

9 Barros D, Takahashi H, Wrasse C M & Figueiredo C A O B, Characteristics of equatorial plasma bubbles observed by TEC map based on ground-based GNSS receivers over South America, *Ann Geophys*, **36(1)** (2018) 91–100.

10 Chapagain N P, Michael J, Taylor Nielsen K & Jarvis M J, Airglow observations and modelling of F region depletion zonal velocities over Christmas Island, *J Geophys Res*, **116(A2)** (2011).

11 Sobral J H A, Abdu M A, Pedersen T R, Vivian M C, Daniela C S A, Muella M T A H, Batista I S, Mascarenhas M, de Paula E R, Kintner P M, Kherani E A, Medeiros A F, Buriti R A, Takahashi H, Schuch N J, Denardini C M, Zamlutti C J, Pimenta A A, de Souza J R & Bertoni F C P, Ionospheric zonal velocities at conjugate points over Brazil during the COPEX campaign: experimental observations and theoretical validations, *J Geophys Res*, **114(A4)** (2009).

12 Yao D & Makela J J, Analysis of equatorial plasma bubble zonal drift velocities in the Pacific sector by imaging techniques, *Ann Geophys*, **25** (2007) 701–709.

13 Adebesin B, Rabiu A, Bolaji O, Adeniyi J & Amory-Mazaudier C, Ionospheric climatology at Africa EIA trough stations during descending phase of sunspot cycle 22, *J Atmos Sol Terr Phys*, **172** (2018) 83–99, https://doi.org/ 10.1016/j.jastp.2018.03.009.

14 Mendillo M & Baumgardner J, Airglow characteristics of equatorial plasma depletions, *J Geophys Res Space Phys*, **87(A9)** (1982) 7641–7652, https://doi.org/10.1029/ ja087ia09p07641.

15 Tsunoda R T, Time evolution and dynamics of equatorial backscatter plumes, I growth phase, *J Geophys Res*, **86(A1)** (1981) 139–149.

16 Woodman R F, Vertical drift velocities and east–west electric fields at the magnetic equator, *J Geophys Res*, **75(31)** (1970) 6249–6259.

17 Chapagain N P, Taylor M J, Makela J J & Duly T M, Equatorial plasma bubble zonal velocity using 630.0 nm airglow observations and plasma drift modeling over Ascension Island, *J Geophys Res Space Phys*, **117(A6)** (2012), https://doi.org/10.1029/2012ja017750.

18 Chapagain N P, Jonathan J M, John W M, Daniel J F, Ricardo A B & Amauri F M, Comparison of nighttime zonal neutral winds and equatorial plasma bubble drift over Brazil, *J Geophys Res*, **117** (2012) A06309.

19 Otsuka Y, Shiokawa K, Ogawa T, Yokoyama T, Yamamoto M & Fukao S, Spatial relationship of equatorial plasma bubbles and field-aligned irregularities observed with an all-sky imager and the equatorial atmosphere radar, *Geophys Res Lett*, **31(20)** (2004).

20 Chapagain N P, Daniel J F, John W M, Chau J L & Jonathan J M, Comparison of zonal neutral winds with equatorial plasma bubble and plasma drift velocities, *J Geophys Res*, **118(4)** (2013) 1802–1812.

21 Fukushima D, Shiokawa K, Otsuka Y, Kubota M, Tsugawa T & Nagatsuma T, Geomagnetically conjugate observation of plasma bubbles and thermospheric neutral winds at low latitudes, *J Geophys Res*, **120(3)** (2015) 2222–2231.

22 Mukherjee G K, Carlo L, Mahayan S H & Patil P T, First results of all-sky imaging from India, *Earth Planets Space*, **50** (1997) 119–127.

23 Chapagain N P, Ionospheric plasma drift and neutral winds modelling, *Res J Phys Sci*, **4(7)** (2016) 5–10.

24 Abdu M A, Outstanding problems in the equatorial ionosphere-thermosphere electrodynamics relevant to spread F, *J Atmos Sol Terr Phys*, **63** (2001) 869–884.

25 Rastogi R G, Seasonal and solar cycle variations of equatorial spread F in the American zone, *J Atmos Sol Terr Phys*, **42(7)** (1980) 593–597.

26 Ajith K K, Ram S T, Yamamoto M, Yokoyama T, Gowtam V S, Otsuka Y, Tsugawa T & Niranjan K, Explicit characteristics of evolutionary-type plasma bubbles observed from equatorial atmosphere radar during the low to moderate solar activity years 2010–2012, *J Geophys Res Space Phys*, **120(2)** (2015) 1371–1382, https://doi.org/10.1002/ 2014ja 020878.

27 Fukao S, Ozawa Y, Yamamoto M & Tsunoda R T, Altitude-extended equatorial spread F observed near sunrise terminator over Indonesia, *Geophys Res Lett*, **30(22)** (2003), https://doi.org/10.1029/2003gl018383.

28 Kelley M C, Larsen M F, LaHoz C & McClure J P, Gravity wave initiation of equatorial spread F: A case study, *J Geophys Res Space Phys*, **86(A11)** (1981) 9087–9100, https://doi.org/10.1029/ja086ia11p09087.

29 Yokoyama T, Fukao S & Yamamoto M, Relationship of the onset of equatorial F region irregularities with the sunset terminator observed with the equatorial atmosphere radar, *Geophys Res Lett*, **31(24)** (2004), https://doi.org/10.1029/ 2004gl021529.

30 Nade D P, Sharma A K, Nikte S S, Patil P T, Ghodpage R N, Rokade M V, Gurubaran S, Taori A & Sahai Y, Zonal velocity of the equatorial plasma bubbles over Kolhapur, India, *Ann Geophys*, **31** (2013) 2077–2084.

31 Shiokawa K, Otsuka Y, Ogawa T & Wilkinson P, Time evolution of high altitude plasma bubbles imaged at geomagnetic conjugate points, *Ann Geophys*, **22(9)** (2004) 3137–3143.

32 Gentile L C, Burke W J & Rich F J, A global climatology for equatorial plasma bubbles in the topside ionosphere, *Ann Geophys*, **24(1)** (2006) 163–172, https://doi.org/10.5194/ angeo-24-163-2006.

33 Huang C S, de La Beaujardiere O, Roddy P A, Hunton D E, Ballenthin J O & Hairston M R, Generation and characteristics of equatorial plasma bubbles detected by the C/NOFS satellite near the sunset terminator, *J Geophys Res*, **117** (2012) A11313.

34 Huang C S, de La Beaujardiere O, Roddy P A, Hunton D E, Ballenthin J O, Hairston M R & Pfaff R F, Large-scale quasiperiodic plasma bubbles: C/NOFS observations and causal mechanism, *J Geophys Res*, **118(6)** (2013) 3602–3612.

35 Immel T J, Frey H U, Mende S B & Sagawa E, Global observations of the zonal drift speed of equatorial plasma bubbles, *Ann Geophys*, **22(9)** (2004) 3099–3107.

36 Karan D K, Eastes R W, Martinis C, Daniell R E, Solomon S C & McClintock W E, Unique combinations of differently shaped equatorial plasma bubbles occurring within a small longitude range, *Earth Space Sci Open Arch*, **(2023)**.

37 Sarudin I, Abdul Hamid N S, Abdullah M, Buhari S M, Shiokawa K, Otsuka Y & Yatini C Y, Equatorial plasma bubble zonal drift velocity variations in response to season, local time, and solar activity across Southeast Asia, *J Geophys Res Space Phys*, **125(3)** (2020), https://doi.org/ 10.1029/2019ja027521.

38 Paulino I, de Medeiros A F, Buriti R A, Takahashi H, Sobral J H A & Gobbi D, Plasma bubble zonal drift characteristics observed by airglow images over Brazilian tropical region, *Ann Geophys*, **29(2)** (2011) 239–246.

39 Nishioka M, Saito A & Tsugawa T, Occurrence characteristics of plasma bubble derived from global ground-based GPS receiver networks, *J Geophys Res*, **113(A5)** (2008).

40 Huang C Y, Burke W H, Machuzak J S, Gentile L C & Sultan P J, Equatorial plasma bubbles observed by DMSP satellites during a full solar cycle: toward a global climatology, *J Geophys Res*, **107(A12)** (2002) 1434.

41 Sahai Y, Kirchhoff V W, Lerne N M & Casiccia C, Total ozone trends in the tropics, *J Geophys Res Atmos*, **105(D15)** (2000) 19823–19828, https://doi.org/10.1029/2000jd900001.

42 Panda S K, Moses M, Ansari K & Walo J, Ionospheric scintillation characteristics over Indian region from latitudinally-aligned geodetic GPS observations, *Earth Sci Inform*, **16** (2023) 2675–2691.

43 Fejer B G, Souza J R, Santos A S & Costa Pereira A E, Climatology of F region zonal plasma drifts over Jicamarca, *J Geophys Res Space Phys*, **110(A12)** (2005), https://doi.org/10.1029/2005ja011324.

44 Cheng K, Huang Y & Chen S, Traveling ionospheric disturbances detected during the solar eclipse of 24 October 1995, *Terr Atmos Ocean Sci*, **8(2)** (1997) 213, https://doi.org/10.3319/tao.1997.8.2.213(asee).

45 Pimenta A A, Bittencourt J A, Fagundes P R, Sahai Y, Buriti R A, Takahashi H & Taylor M, Ionospheric plasma bubble zonal drifts over the tropical region: a study using OI 630 nm emission all-sky images, *J Atmos Sol Terr Phys*, **65(10)** (2003) 1117–1126.

46 Sharma A K, Nade D P, Nikte S S, Patil P T, Ghodpage R N, Vhatkar R S, Rokade M V & Gurubaran S, Occurrence of equatorial plasma bubble over Kolhapur, *Adv Space Res*, **54** (2014) 435–442.

47 Tsunoda R T, Control of the seasonal and longitudinal occurrence of equatorial scintillations by the longitudinal gradient in integrated E region Pedersen conductivity, *J Geophys Res Space Phys*, **90(A1)** (1985) 447–456, https://doi.org/10.1029/ja090ia01p00447.

48 Aarons J, Global morphology of ionospheric scintillations, *Proc IEEE*, **70(4)** (1982) 360–378, https://doi.org/10.1109/ proc.1982.12314.

49 Buhari S M, Abdullah M, Yokoyama T, Otsuka Y, Nishioka M, Hasbi A M, Bahari S A & Tsugawa T, Climatology of successive equatorial plasma bubbles observed by GPS ROTI over Malaysia, *J Geophys Res*, **122(2)** (2017) 2174–2184.

50 Saito S & Maruyama T, Large-scale longitudinal variation in ionospheric height and equatorial spread F occurrences observed by ionosondes, *Geophys Res Lett*, **34(16)** (2007), https://doi.org/10.1029/2007gl030618.

51 Nade D P, Sharma A K, Nikte S S, Ghodpage R N, Patil P T, Rokade M V & Vhatkar R S, Occurrence of F-region plasma bubble over low latitude station: Kolhapur, *Proc CARCAN*, **(2012)** 94–99.

52 Burke W J, Gentile L C, Huang C Y, Valladares C E & Su S Y, Longitudinal variability of equatorial plasma bubbles observed by DMSP and ROCSAT-1, *J Geophys Res Space Phys*, **109(A12)** (2004), https://doi.org/10.1029/ 2004j a010583.

53 de Paula E R, Kantor I J, Sobral J H A, Takahashi H, Santana D C, Gobbi D, Medeiros A F, Limiro L A T, Kil H, Kintner P M & Taylor M J, Ionospheric irregularity zonal

velocities over Cachoeira Paulista, *J Atmos Sol Terr Phys*, **64(12–14)** (2002) 1511–1516.

54 Fejer B G, F-region plasma drifts over Arecibo: solar cycle, seasonal, and magnetic activity effects, *J Geophys Res Space Phys*, **98(A8)** (1993) 13645–13652, https://doi.org/10.1029/93ja00953.

55 Fejer B G & Scherliess L, Mid- and low-latitude prompt-penetration ionospheric zonal plasma drifts, *Geophys Res Lett*, **25(16)** (1998) 3071–3074, https://doi.org/10.1029/98gl02325.

56 Otsuka Y, Shiokawa K & Ogawa T, Equatorial ionospheric scintillations and zonal irregularity drifts observed with closely spaced GPS receivers in Indonesia, *J Meteorol Soc Jpn*, **84A** (2006) 343–351.

57 Yokoyama T & Fukao S, Upwelling backscatter plumes in growth phase of equatorial spread F observed with the equatorial atmosphere radar, *Geophys Res Lett*, **33(8)** (2006).

58 Immel T J, Mende S B, Frey H U, Peticolas L M & Sagawa E, Determination of low latitude plasma drift speeds from FUV images, *Geophys Res Lett*, **30(18)** (2003).

59 Terra P M, Sobral J H A, Abdu M A, Souza J R & Takahashi H, Plasma bubble zonal velocity variations with solar activity in the Brazilian region, *Ann Geophys*, **22(9)** (2004) 3123–3128.

60 Huang C & Roddy P A, Effects of solar and geomagnetic activities on the zonal drift of equatorial plasma bubbles, *J Geophys Res Space Phys*, **121(1)** (2016) 628–637, https://doi.org/10.1002/2015ja021900.

61 Carmo C S, Dai L, Denardini C M, Figueiredo C A, Wrasse C M, Resende L C, Barros D, Moro J, Chen S S, Picanço G A, Silva R P, Wang C, Li H & Liu Z, Equatorial plasma bubbles features over the Brazilian sector according to the solar cycle and geomagnetic activity level, *Front Astron Space Sci*, **10** (2023), https://doi.org/10.3389/fspas.2023.1252511.

62 Han C, Li G, Sun W, Xie H, Hu L & Zhao X, Generation and evolution of post-sunset equatorial plasma bubbles in east and Southeast Asia during the July 2022 geomagnetic storm, *Adv Space Res*, **73(3)** (2024) 1843–1853, https://doi.org/10.1016/j.asr.2023.10.046.

63 Haerendel G, Eccles J V & Cakir S, Theory for modeling the equatorial evening ionosphere and the origin of the shear in the horizontal plasma flow, *J Geophys Res*, **97(A2)** (1992) 1209–1223.

64 Portella V N, Altadill D, Blanch E, Altadil M, Segarra A, Paula V D, Timoté C C & Juan J M, Estimation of the drift velocity of Equatorial Plasma Bubbles using GNSS and digisonde data, *J Space Weather Space Clim*, **15(2)** (2025), https://doi.org/10.1051/swsc/2024038